Journal of the Energy Institute 110 (2023) 101355

Contents lists available at ScienceDirect

Journal of the Energy Institute

journal homepage: www.elsevier.com/locate/joei

Low-temperature chemical looping oxidation of hydrogen for space heating

Fatih Güleç [a,b,*], Jude A. Okolie [c], Peter T. Clough [d], Ahmet Erdogan [a,e], Will Meredith [b], Colin E. Snape [b]

[a] Advanced Materials Research Group, Department of Chemical and Environmental Engineering, Faculty of Engineering, University of Nottingham, Nottingham, NG7 2RD, UK
[b] Low Carbon Energy and Resources Technologies Research Group, Faculty of Engineering, University of Nottingham, Nottingham, NG7 2TU, UK
[c] Gallogly College of Engineering, University of Oklahoma, Norman, 73019, USA
[d] Energy and Sustainability Theme, Cranfield University, Cranfield, Bedfordshire, MK43 0AL, UK
[e] Mechanical Engineering, Faculty of Engineering, Inonu University, 44280, Malatya, Turkey

ARTICLE INFO

Handling Editor: Dr. Paul Williams

Keywords:
Advanced combustion
Chemical looping combustion (CLC)
Hydrogen
Oxygen carriers

ABSTRACT

Chemical looping combustion (CLC) is an advanced combustion process in which the combustion reaction splits into two parts; in the first reaction metal oxides are used as oxygen suppliers for fuel combustion and then in the second reaction, reduced metal oxides are re-oxidised in an air reactor. Although this technology could be applicable for the safe implication of "low-temperature oxidation of hydrogen", there is limited understanding of oxygen carrier reduction stages and the oxidation mechanism of hydrogen throughout the process. The novelty of this research lies in its pioneering investigation of low-temperature oxidation of hydrogen through chemical looping technology as a safe and alternative heating system, using three distinct metal oxide oxygen carriers: CuO, Co_3O_4, and Mn_2O_3. The oxidation of hydrogen over these oxygen carriers was comprehensively studied in a fixed-bed reactor operating at 200–450 °C. XRD analysis demonstrates that CuO directly reduced to metallic Cu at 200–450 °C, instead of following a sequential reduction step $CuO \rightarrow Cu_4O_3 \rightarrow Cu_2O \rightarrow Cu$ throughout the temperature. Co_3O_4 was reduced to a mixture CoO and Co at 450 °C, which may refer to a sequential reduction step $Co_3O_4 \rightarrow CoO \rightarrow Co$ with increasing the temperature. Decreasing the reduction temperature led to an elevation in CoO formation. Mn_2O_3 can also reduce to a mixture of Mn_3O_4 and MnO at temperatures between 250 and 400 °C. Compared to temperature, the increase in the residence time did not show any further reduction in Mn_2O_3. SEM results showed that most of the metal oxide particles were evenly dispersed on the supports. Based on the experimental results, a potential reduction stage of CuO, Co_3O_4 and Mn_2O_3 was proposed for low-temperature hydrogen oxidation, which could be a potential application for space heating using safe hydrogen combustion.

1. Introduction

The present world is faced with challenges such as greenhouse gas (GHG) emissions, environmental pollution, and climate change. These challenges arise due to the elevating human population resulting from rapid industrialization, urbanization, and commercialization. As one of the most lethal anthropogenic greenhouse gases, CO_2 emissions have reached alarming levels [1]. The heating of industrial, domestic, and commercial buildings accounts for a third of the UK greenhouse gas emissions, with about half coming from domestic space and water heating (Squires; and Goater;, 2016). The majority of households (88%) own natural gas boilers despite the high CO_2 emissions. In comparison to the CO_2 emission limit for domestic heat set by the Committee on Climate Change for 2030 (180 gCO_2eq/kWh), natural gas boilers have an average carbon footprint of around 300 gCO_2eq/kWh [2].

In the gas boilers, combustion of the gas releases thermal energy for heating water, which is used for water and space heating. There are alternatives based on their energy sources, such as heat pumps, biomass, electric, and hydrogen boilers. The principle of electric boilers is similar to that of conventional gas boilers, but they use electricity to generate heat directly. Based on the levelised cost of energy (LCOE), electric heating is second-cheapest after gas boilers [3]. A heat pump transfers thermal energy in the opposite direction to spontaneous heat transfer, by absorbing heat from a cold space and releasing it into a warmer space.

* Corresponding author. Advanced Materials Research Group, Department of Chemical and Environmental Engineering, Faculty of Engineering, University of Nottingham, Nottingham, NG7 2RD, UK.
E-mail address: Fatih.Gulec1@nottingham.ac.uk (F. Güleç).

https://doi.org/10.1016/j.joei.2023.101355
Received 27 January 2023; Received in revised form 25 July 2023; Accepted 1 August 2023
Available online 2 August 2023

Heat pumps have a carbon footprint of around 90–190 gCO_2eq/kWh based on the efficiency of the boiler [2]. The carbon footprint of heat pumps is also affected by the amount of electricity used, but they are more efficient than electric boilers since they have a coefficient of performance greater than 1.0. A biomass boiler is a heating system that burns biomass, such as wood, straw, crops, and agricultural wastes. It is possible to reduce CO_2 emissions significantly by using biomass boilers and to reach net-zero emissions, but since biomass has a low calorific value and a low energy density, the efficiency is rather low. Additionally, biomass is characterised by a low combustion efficiency (minimum is set as 75–77% by the UK government) and high moisture content [4]. But the efficiency can considerably vary based on the fuel quality (Georgina Orr, 2018). Using biomass boiler instead of gas boiler may results up to 73–90% of emission saving [5]. Although, the requirement of extra care is disadvantage, a maintenance program could be set for weekly basis to clean the boiler and remove ashes (Georgina Orr, 2018). Additionally, the LCOE of the biomass boiler (~€106/MWh) is higher than natural gas boilers (~€53/MWh) [3].

Considering the developments of hydrogen production technologies, hydrogen boilers are receiving greater attention in order to fulfilling net-zero CO_2 emission in space heating systems. Comparing the other energy sources, hydrogen is one of the most environmentally friendly energy source as it release heat and water as by product with a high combustion efficiency [6]. Hydrogen is therefore considered an energy vector in domestic and industrial applications [7]. The developments of hydrogen boilers in which hydrogen operates safely are therefore significantly important to reach a net-zero future for space heating. As historically, syngas containing 50% hydrogen was in part adopted as a town gas used for street lighting, cooking, and domestic heating [8]. The design and development of hydrogen-powered technologies and systems, including internal combustion engines, fuel cells, and heating systems, are of great interest. Researchers have shown that typically, hydrogen is burned in the air, resulting in significant amounts of nitrogen oxides, which contribute to greenhouse gas emissions, acid rain, and smog [9].

Therefore, hydrogen combustion safety must be taken into consideration when designing a space heating system that uses hydrogen. Direct air hydrogen combustion has some challenges related to the emissions [10], previous studies have shown that the direct combustion of hydrogen in the air has some undesirable effects such as flash-backs (an explosion caused by a flame entering the area from which the hydrogen was supplied) and increased formation of NO_x [11,12]. The novelty of this research lies in its pioneering investigation of low-temperature oxidation of hydrogen through chemical looping technology, using three distinct metal oxide oxygen carriers: CuO, Co_3O_4, and Mn_2O_3. Spent FCC catalyst particles are used as cheap oxygen carrier supports in this application. The oxidation of hydrogen over these oxygen carriers was investigated in a fixed bed reactor operating at 200–450 °C. The comprehensive characterisation of the oxygen carriers and their behaviour before and after hydrogen oxidation valuable insights into the reduction stages of metal oxides. By proposing a potential reduction stage for each oxygen carrier, this research paves the way for the practical implementation of low-temperature chemical looping as a safe and efficient method for hydrogen combustion for space heating.

2. Chemical looping oxidation of hydrogen

Low-temperature chemical looping combustion (CLC) could be one of the potential technologies as for the future's new hydrogen boilers to eliminate the problems rase through direct hydrogen combustion. The hydrogen chemical looping oxidation (CLO-H_2) involves the utilization of two series reactions; hydrogen oxidation in a fuel reactor and metal oxidation in an air reactor, which can be operated as interconnected fluidised bed reactors or parallel fixed bed reactors (Fig. 1).

In the air reactor, the reduced form of metal oxides (i.e. Cu) is re-

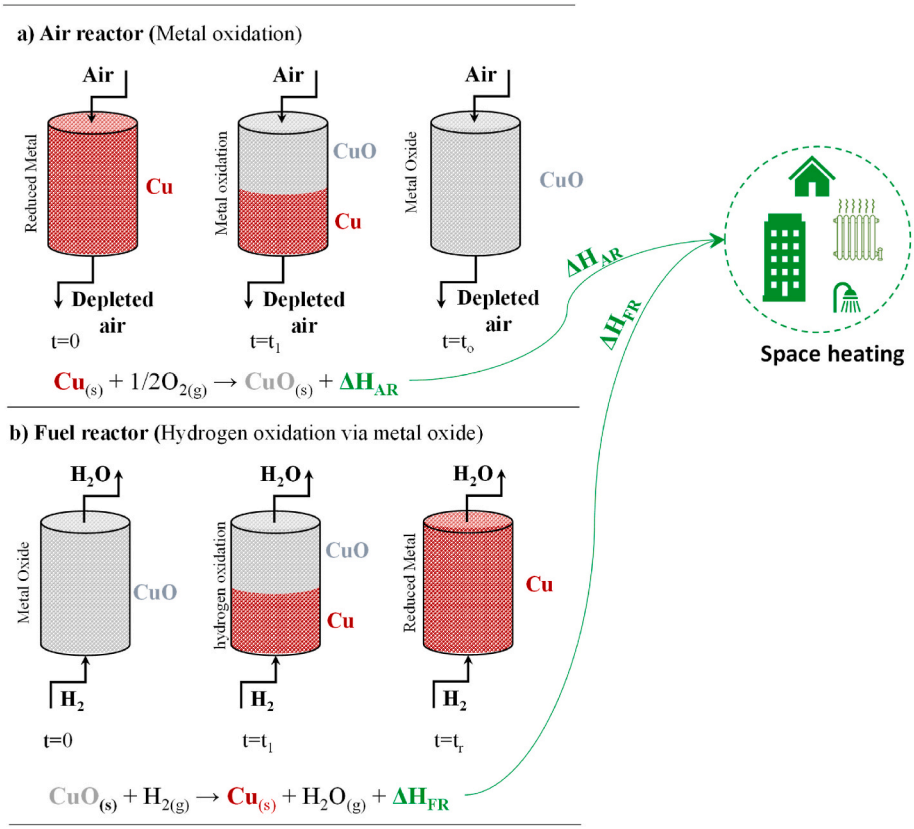

Fig. 1. Chemical looping oxidation of hydrogen for space heating: a) Metal oxidation in air reactor (t_o represents the time required for the oxidation of reduced metals), b) Hydrogen oxidation with metal oxide in fuel reactor (t_r represents the metal oxide reduction time).

oxidised (i.e. CuO) by the oxygen in air stream (R1). The fuel reactor is where the hydrogen oxides by metal oxide (i.e. CuO) to H_2O while metal oxides (i.e.CuO) are reduced to metal form (i.e. Cu, R1) at a low temperature [13]. The reduced metal can be then reused in oxidation in air reactor, which makes this process looping and produce energy. The energy produced in the air reactor can be extracted by a water flow, which can operate space heating systems.

$$\text{Air Reactor}: Cu_{(s)} + O_{2(g)} \rightarrow CuO_{(s)} \quad \Delta H^{o}_{rxn,AR} = -155.2\ \text{kJ} \Big/ \text{mol} \qquad \text{(R1)}$$

$$\text{Fuel Reactor}: CuO_{(s)} + H_{2(g)} \rightarrow Cu_{(s)} + H_2O_{(g)} \quad \Delta H^{o}_{rxn,FR} = -130.8\ \text{kJ} \Big/ \text{mol} \qquad \text{(R2)}$$

$$\text{Net Reaction}: H_{2(g)} + O_2 \rightarrow H_2O_{(g)} \quad \Delta H^{o}_{rxn} = -286.0\ \text{kJ} \Big/ \text{mol} \qquad \text{(R3)}$$

Where; $\Delta H^{o}_{rxn,AR}$ and $\Delta H^{o}_{rxn,FR}$ represents the reactions standard heats for the metal oxide oxidation in air reactor and hydrogen oxidation in fuel reactor at 1 atm *and 298 K ΔH^{o}_{rxn} is the standard heats of net reaction (hydrogen oxidation).*

Low-temperature CLC has been proposed as a novel technology to eliminate uncombusted hydrocarbon gases, non-methane volatile organic compounds, and CO released from incomplete biofuel and coal combustion [14–16]. As these incomplete combustion gases clearly decrease the combustion efficiency [17,18]. Co-combustion of coal with peach and apricot stones as industrial waste was investigated using a bubbling fluidised bed [17]. The increase in the biomass content in the fuel mixture increase the CO and uncombusted hydrocarbon emissions due to the catalytic reduction of CO and uncombusted hydrocarbons in the flue gas thanks to the high volatile contents of biomass [17]. Low-temperature CLC concept has been proposed to attain complete combustion which means higher combustion efficiency, higher CO_2 purity in the flue gas and much lower toxic hydrocarbon gas emissions in the industrial process. The use of interconnected fluidised beds introduces substantial complexity and cost to the process. Alternatively, a fixed bed designed with an alternating gas flow for synchronised operation is proposed [19].

Although the chemical looping technology can also be a potential application for the safe implication of "low-temperature oxidation of hydrogen", there is limited understanding of oxygen carrier reduction mechanisms and oxidation mechanism of hydrogen, which is significantly important for the long-term application of low-temperature oxidation of hydrogen via chemical looping and process design. In this study, a brief overview of the applicability of low-temperature oxidation of hydrogen with chemical looping technology has been experimentally investigated using a wide range of oxygen carriers and low-temperature process conditions. The reduction mechanisms of oxygen carriers and the oxidation mechanism of hydrogen were identified using comprehensive material characterisation techniques.

3. Materials and methods

3.1. Preparation of oxygen carriers

In order to synthesise the oxygen carriers, a wet-impregnation method was used with Cu-, Co- and Mn- based nitrates as precursors of metal oxides and spent Fluid Catalytic Cracking (FCC) catalyst (equilibrium catalyst supplied by Chemical Process and Energy Resources Institute – CPERI) as support [20,21]. The oxygen carriers preparation steps are as follows; 25 ml aqueous solution of Co $(NO_3)_2.6H_2O$, $Cu(NO_3)_2.3H_2O$, and $Mn(NO_3)_2.4H_2O$ and were prepared using distilled water. 20 g of used FCC supports were then slowly added into the metal solutions at 25 °C and impregnated for 18 h. Following the metal modified FCC supports dried at 60 °C (24 h) and 100 °C (4 h), the samples were calcined at 550 °C for 30 min using air where nitrate salts were decomposed into CuO, Co_3O_4, and Mn_2O_3. The oxidised form metal oxides modified FCC supports were designated as Mn_2O_3/FCC (29.8 wt % of Mn_2O_3), Co_3O_4/FCC (17.8 wt % of Co_3O_4), and CuO/FCC (12.5 wt % of CuO).

3.2. CLC of hydrogen in a lab-scale fixed bed

In order to investigate and characterise the oxygen carriers after the hydrogen oxidation, the reduction tests of spent FCC catalysts supported oxygen carriers (CuO/FCC, Co_3O_4/FCC, and Mn_2O_3/FCC) were also performed using hydrogen in a fixed bed unit. Schematics of the fixed bed unit is presented in Fig. 2. Firstly, 5 g of prepared oxygen carriers (CuO/FCC, Co_3O_4/FCC, or Mn_2O_3/FCC) was placed in the tubular reactor having a 9 mm of diameter and 25 cm of length. The samples was then heated from 25 °C to target temperature (200, 250, 300, 350, and 450 °C) with 20 °C/min and kept at the target temperature for 1 h under a hydrogen flow rate of 30 ml/min and a pressure of 5 bar.

3.3. Characterizations of prepared and tested oxygen carriers

Spent FCC catalysts supported oxygen carriers (metal oxides) were characterised using a wide range of techniques in order to identify the physio-chemical structures of metal oxides before and after hydrogen oxidation.

3.3.1. XRD analysis

Crystalline phases before and after each hydrogen oxidation were measured using a X-ray powder diffractometer (XRD, Siemens D500) using Cu-Kα at 40 kV and 35 mA. Each sample (CuO/FCC, Co_3O_4/FCC, and Mn_2O_3/FCC) was scanned over a $2\theta = 30°–60°$ with 0.05° as step size and 2 s as step time. Joint Committee on Powder Diffraction Standards (JCPDS) were used to correlate the XRD results.

3.3.2. SEM and EDS analysis

The surface morphology, agglomeration, and sintering of metal

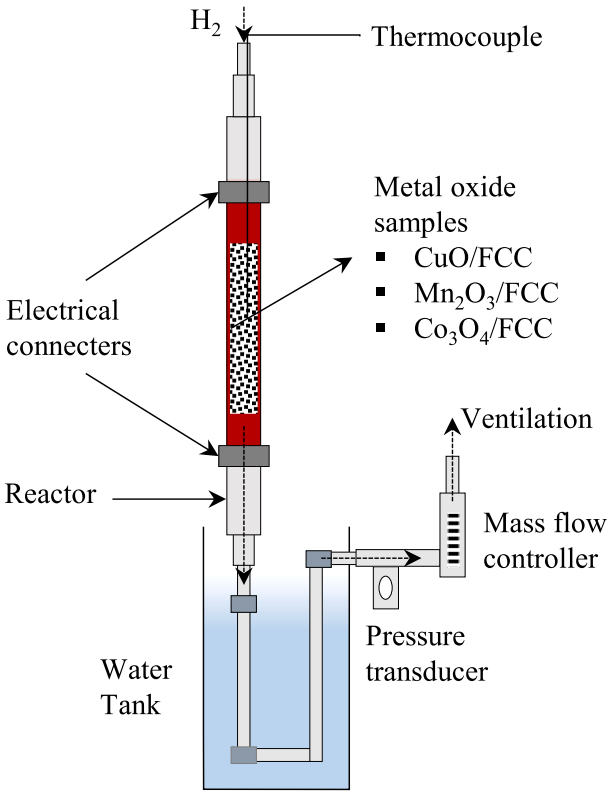

Fig. 2. Fixed-bed unit used for hydrogen oxidation tests.

oxide modified FCC supports (and the samples after hydrogen oxidation) were measured using a secondary electron imaging (SEI) mode of Scanning Electron Microscope (SEM, JEOL JSM 6490LV) based on three different magnifications of 20, 10, and 1 μm at 20 kV accelerated voltage. Additionally, the elemental characterisation, especially the distribution of impregnated oxygen carriers on spent FCC catalysts has been identified by Energy-Dispersive X-ray Spectroscopy (EDS) mapping and spectrums using Oxford X-Max spectroscopy. The qualitative elemental analysis of the oxygen carrier impregnated FCC supports was identified using spot mode in which the beam is focused on a specified area or point manually chosen by the researcher in the field of view. The selected locations are presented on the SEM images with using a square (□) or a plus sign (+).

3.3.3. N_2 adsorption-desorption analysis

The surface and pore structures of oxygen carriers modified on FCC supports were measured by N_2 sorption analysis using a Micromeritics ASAP 2420 (Micromeritics). Prior to analysis, moisture and adsorbed gases were removed using the following procedure: ~0.2 g of metal oxide samples was degassed at 150 °C for 15 h under vacuum. Nitrogen isotherms have measured with a range from 0.01 to 0.99 of relative pressures (P/P°) at −196 °C in liquid nitrogen. The Brunauer, Emmett, and Teller (BET) and Barrett, Joyner, and Halenda (BJH) methods were used to determine the specific surface area and pore volume using Microactive Software V3.0. Furthermore, the pore volume and surface area were determined using t-Plot, which is the most common method to measured external surface area and micropore volume of metal oxide modified FCC supports.

3.3.4. XRF analysis

The quantity of oxygen carrier impregnated on spent FCC catalysts was analysed by X-ray fluorescence (XRF, Panalytical Epsilon 3-XL). The samples having a powder form were filled in a pot having a diameter of 27 mm. A thin Prolene film having a thickness of 4.0 μm placed at the bottom of the pot, allowed for the X-rays to quantitatively measure the elemental composition of the samples using a 40 kV Ag-anode X-ray tube, calibrated by internal Omnion calibration programme.

3.3.5. True density analysis

The true density of metal oxides (oxygen carriers, before and after reduction) were measured using a Micromeritics AccuPyc II 1340 Gas Pycnometer. The equipment is a gas displacement pycnometer measuring the pore volume of the solid samples by differences of the volume of sample chamber and expansion chamber which was modified by the ratio of gauge pressure after fill and expansion. The volumes used in the calculation were measured with helium using a sample holder having a volume of 1 cm^3. The true density of oxygen carriers was determined by the ratio of mass to volume of metal oxide modified FCC particles.

4. Results and discussion

4.1. Crystalline phases before and after hydrogen combustion

The XRD patterns of Spent FCC, CuO/FCC before and after hydrogen oxidation at different temperatures is presented in Fig. 3. The presence of strong peaks at 35.5°, 38.6°, and 48.8° on the CuO/FCC in the figure prove that CuO (JCPDS no: 01-080-0076) was successfully impregnated into the matrix and fillers of spent FCC catalysts. The XRD patterns of CuO/FCC reduction states by hydrogen at 450, 250 and 200 °C are also presented in Fig. 3. The characteristic peaks of Cu; 43.3° and 50.4° (JCPDS no: 01-085-1326) were observed for the samples reduced by hydrogen at the temperatures between 200 and 450 °C. The CuO directly reduce to Cu, instead of following a sequential reduction step CuO → Cu_4O_3 → Cu_2O → Cu. This is because there was no hint showing the characteristic peaks for neither Cu_4O_3 nor Cu_2O in Fig. 3. The CuO reduction stage was to Cu_2O once CO was used as a reduction gas at the isothermal reduction temperature of 250 °C [22].

Fig. 4 demonstrates the reduction states of Co_3O_4, which was impregnated on spent FCC catalysts depending on the temperatures. The sharp peaks at 31.2°, 36.8°, 38.5°, and 44.8° on the Co_3O_4/FCC demonstrate the successful impregnation of Co_3O_4 (JCPDS no: 00-042-1467) on spent FCC catalysts. Co_3O_4 was reduced to CoO and Co at 450 °C, which may refer to a sequential reduction step Co_3O_4→CoO→Co. The Co formation was decreased, and so the CoO formation was increased with a decrease in the reduction temperatures from 450 °C to 350 °C. However, unreduced oxygen carriers, Co_3O_4, was observed (Fig. 4) when the reduction temperature was under 300 °C. The further decrease in the reduction temperature caused a decrease in the reduction (Fig. 4), where the Co_3O_4 peaks were more intense. Ward et al. [23] observed that although the majority of the crystals are in the form of Co_3O_4, the formation of CoO has been beginning at the temperatures around 250 °C. The distribution of Co-states was determined using semi quantification method and presented in Table 1.

The characteristic peaks at 23.1°, 32.9°, 38.2°, 45.1°, 49.3°, and 53.2° on the Mn_2O_3/FCC in Fig. 5 prove the successful impregnation of

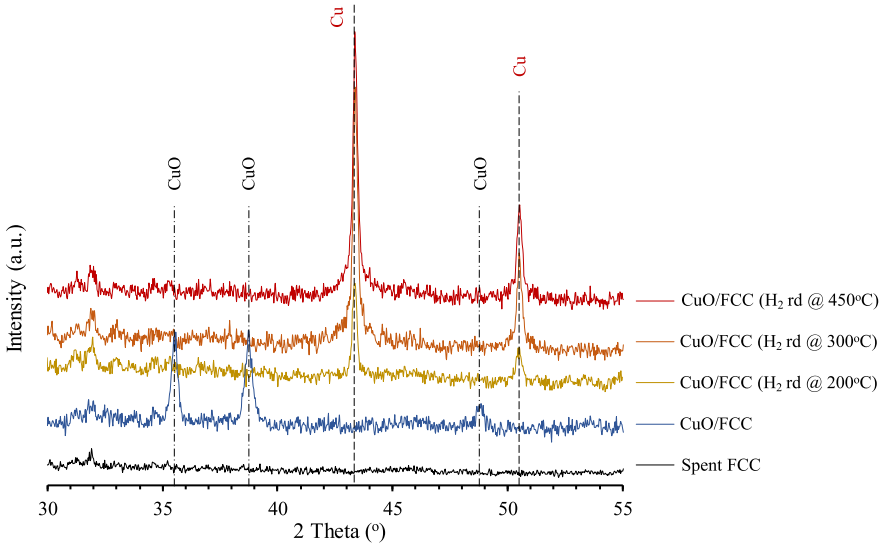

Fig. 3. XRD patterns of Spent FCC, CuO/FCC before and after hydrogen oxidation at 200, 300, 450 °C.

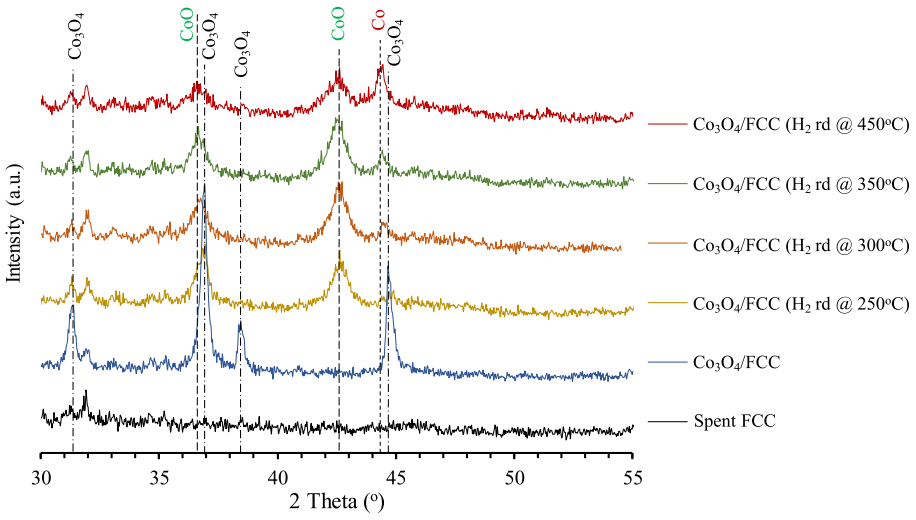

Fig. 4. XRD patterns of Spent FCC, Co_3O_4/FCC before and after hydrogen oxidation at 250, 300, 350, 450 °C.

Table 1
Cu-, Co- and Mn-states after reduction of CuO/FCC, Co_3O_4/FCC, and Mn_2O_3/FCC**.

T_r[a] (°C)	Cu-states, wt. %			Co-states, wt. %			Mn-states, wt. %		
	CuO	Cu_2O	Cu	Co_3O_4	CoO	Co	Mn_2O_3	Mn_3O_4	MnO
450	–	–	100	–	14.9	85.1	–	–	100
350	–	–	100	–	80.2	19.8	6.3	8.9	84.8
300	n.a.	n.a.	n.a.	27.0	61.7	11.3	19.1	79.0	1.9
250	–	–	100	45.3	53.4	–	19.0	81.0	–

[a] Reduction temperature of oxidised oxygen carriers under H_2 atmosphere at 5 bar ** The ratios presented in Table 1 are determined by semi-quantification method. "n.a." refers non-applicable, as the reduction of CuO with H_2 at 300 °C has not been investigated.

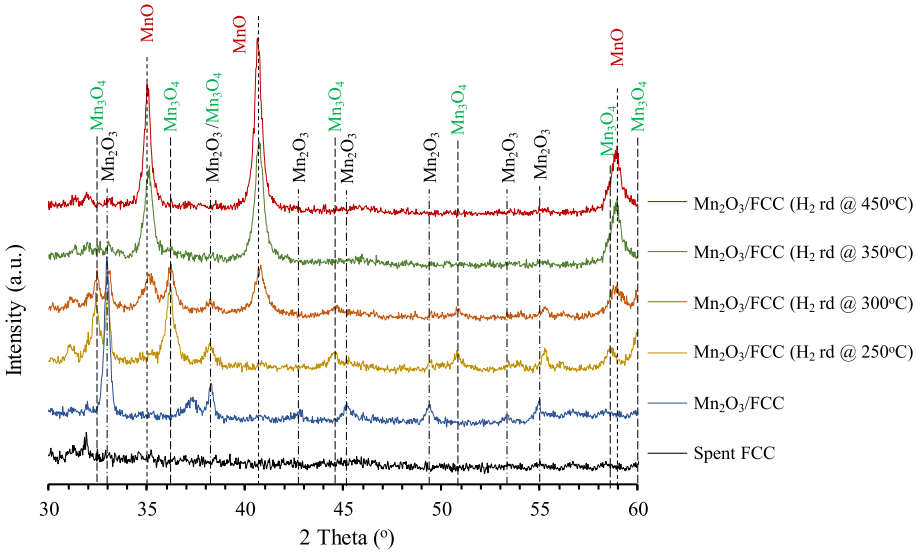

Fig. 5. XRD patterns of Spent FCC, Mn_2O_3/FCC before and after hydrogen oxidation at 250, 300, 350, 450 °C.

Mn_2O_3 (JCPDS no: 01-071-0636) on spent FCC catalysts. As for the reduction results, Mn_2O_3 can directly reduce to MnO, representing the characteristic 2θ peaks at 34.9°, 40.5°, and 58.7° (JCPDS no: 01-078-0424) at 350 and 450 °C (Fig. 5). However, once the temperature was lower than 300 °C, a second step of the sequential reduction, $Mn_2O_3 \rightarrow Mn_3O_4 \rightarrow MnO$, can be observed (at 250 and 300 °C). The additional reduction on Mn_2O_3 was attributed to Mn_2O_3 dispersion over the surfaces of FCC support resulting from the wet-impregnation method. As the second step of the sequential reduction, $Mn_3O_4 \rightarrow MnO$, is defined as rate limiting once the Mn_2O_3 is in the form of 'bulk' [21] while it is faster once Mn_2O_3 impregnated on spent FCC catalyst. The distribution of Mn-states was also determined using semi quantification method and presented in Table 1.

Fig. 6 shows that the effects of residence time (1.0, 1.5, and 2.0 h) on the reduction of metal oxides (Mn_2O_3/FCC) in the hydrogen atmosphere under isothermal conditions (250 °C). Compared to temperature, the increase in the residence time did not show any further reduction on Mn_2O_3/FCC. Regardless of the residence time, Mn_2O_3 only reduced to

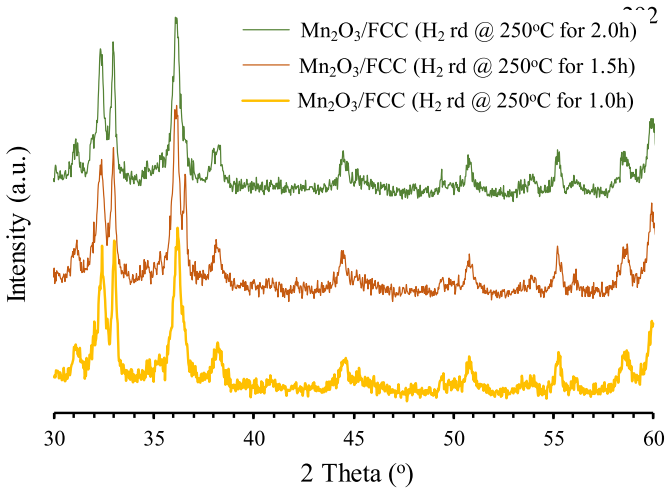

Fig. 6. XRD patterns of Mn_2O_3/FCC after hydrogen oxidation at 250 °C for 1.0, 1.5, and 2.0 h.

Mn_3O_4 at the reduction temperature of 250 °C under hydrogen atmosphere.

4.2. Surface analysis before and after hydrogen combustion

SEM was employed to investigate any deformation on the surface morphology and physical structure of spent FCC particles after impregnation of oxygen carriers and testing in the hydrogen oxidation. Fig. 7 demonstrates the surface morphology of spent FCC in three different zoom scaling, 20 μm, 10 μm, and 1 μm. The figure indicates that the spent FCC catalysts have a spherical shape and smooth surface.

The SEM images of both CuO/FCC and Cu/FCC (at 350 °C) at the three different scales (20, 10, 2 μm) are presented in Fig. 8a and b, respectively. There is no evidence showing fragmentation or any physical deformation on FCC particles after the impregnation of CuO (13 wt %) as seen from Fig. 8a, neither after it reduced to Cu/FCC by hydrogen (Fig. 8b) at 350 °C. The CuO particles were mostly dispersed on the surface of spent FCC supports. However, the bright points in Fig. 8a and b, corresponds to the accumulation of CuO and Cu on the FCC support. Similarly CuO accumulation on Al_2O_3 was reported due to the impregnation method [24]. The increase in the content of CuO may elevate the surface accumulation as seen on the FCC surface [24,25]. Furthermore, very little agglomeration between the spherical CuO impregnated FCC particles was observed. The accumulated CuO on one FCC particle is connected with CuO impregnated on another FCC particle, which enables agglomeration.

The spherical FCC particles demonstrate fragmentation into smaller particles after the impregnation of Co_3O_4 (18 wt %) (Fig. 9a). Additionally, an oxygen carrier accumulation on prepared Co_3O_4/FCC has clearly been observed in Fig. 9a (10-2 μm). This accumulation may be attributed to the high amount of Co_3O_4 impregnated on the support (FCC). On the other hand, no significant differences on the surface of Co_3O_4/FCC were observed between fresh and used in hydrogen oxidation at 350 °C.

As for the impregnation of Mn_2O_3 on spent FCC catalyst, the spherical FCC particles demonstrate quite significant fragmentation into smaller particles following the impregnation of Mn_2O_3 (30 wt %), as seen Fig. 10a. Additionally, the smooth surface of the FCC particles was fully covered by Mn_2O_3. In terms of both Mn_3O_4/FCC (Fig. 10b) and MnO/FCC (Fig. 10c), the oxygen carriers demonstrated similar properties such as fragmentation, agglomeration and Mn-based accumulation due to the fact that both were prepared by the reduction of Mn_2O_3/FCC with hydrogen. As shown previously (Fig. 10a), FCC demonstrates remarkable fragmentation, agglomeration and Mn- accumulation after the impregnation of Mn_2O_3. Thus, these deformations came also forward on its reduced forms, both MnO/FCC and Mn_3O_4/FCC.

To clarify the agglomeration of Mn_2O_3/FCC, SEM image and EDS spectrums have been investigated on a lump of FCC particles and presented in Fig. 11. The SEM image of the agglomerated part of Mn_2O_3/FCC showed that the space between FCC particles labelled 1 and 2 seem different than the FCC catalyst surface labelled 3 and 4. EDS spectrums of 1 and 2 show that the oxygen carrier (Mn_2O_3) is stacking the FCC particles, which cause the agglomeration. Furthermore, the EDS spectrums for 3 and 4 demonstrate that although the oxygen carriers cover the outer surface of FCC particles, the other elements such as Si, Al, and La, can still be detectable. It can be concluded that the FCC support pores are still accessible, which is important to keep the pores accessible for hydrogen combustion.

Moreover, agglomeration between Mn_2O_3 impregnated FCC particles can clearly be observed from Fig. 10 due to the high amount of Mn_2O_3 accumulation on the outer surface of FCC particles. However, similar to CuO and Co_3O_4 impregnated FCC supports, significant differences on the surface of fresh Mn_2O_3/FCC were not observed when compared with the catalysts tested after the hydrogen oxidation. As reported by Bhan and Delgass [26], Me^{3+} cations are located preferentially on the outer surface of ZSM-5 zeolite, whereas Me^{2+} cations are located inside the zeolite. Similar findings have also been reported as the ZSM-5 zeolite catalyst modified by ZnO, CuO as Me^{2+} and Ga_2O_3 as Me^{3+} [27]. Thus, the oxygen carrier accumulation on FCC may be attributed to the impregnated metal's cation states as well as the quantity of oxygen carriers used for the impregnation. This is in line with our results where less accumulation was observed on the outer surface of Cu^{2+} impregnated FCC support (Fig. 8a) compared with Mn^{3+} impregnated FCC support (Fig. 10a). Furthermore, the accumulation of Co_3O_4 impregnated FCC particle is more than CuO/FCC while it is less than Mn_2O_3/FCC. This may be attributed to the cation states of Co_3O_4, which has both Co^{2+} and Co^{3+}. As the Co^{2+} cations diffuse into the pores while the Co^{3+} cations were mostly accumulated outer surface of FCC particles.

4.3. XRF and EDS mapping of oxygen carriers before and after reduction

The quantity of oxidised metal oxides, Mn_2O_3, CuO, and Co_3O_4 and

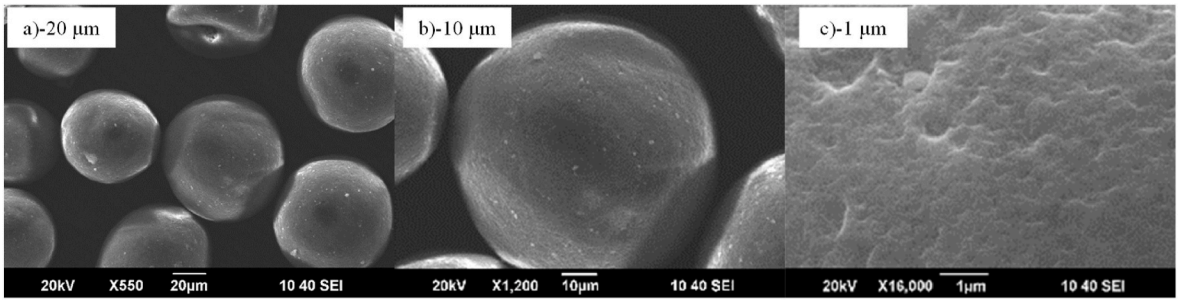

Fig. 7. SEM images of Spent FCC.

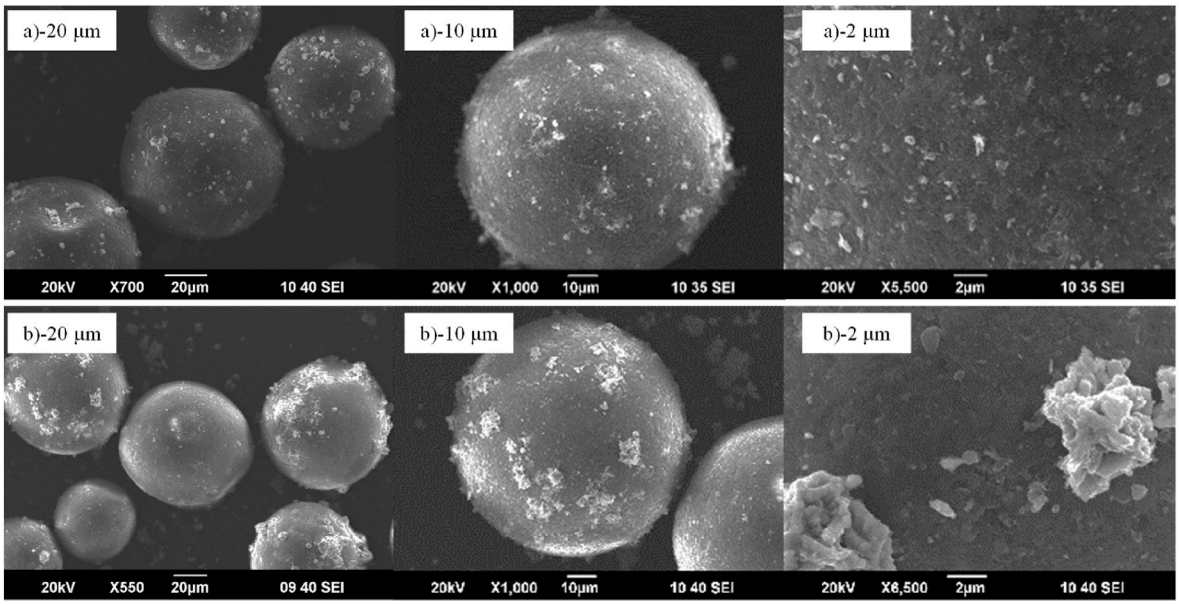

Fig. 8. SEM images of a) CuO/FCC and b) after hydrogen oxidation with CuO/FCC at 350 °C (Cu/FCC).

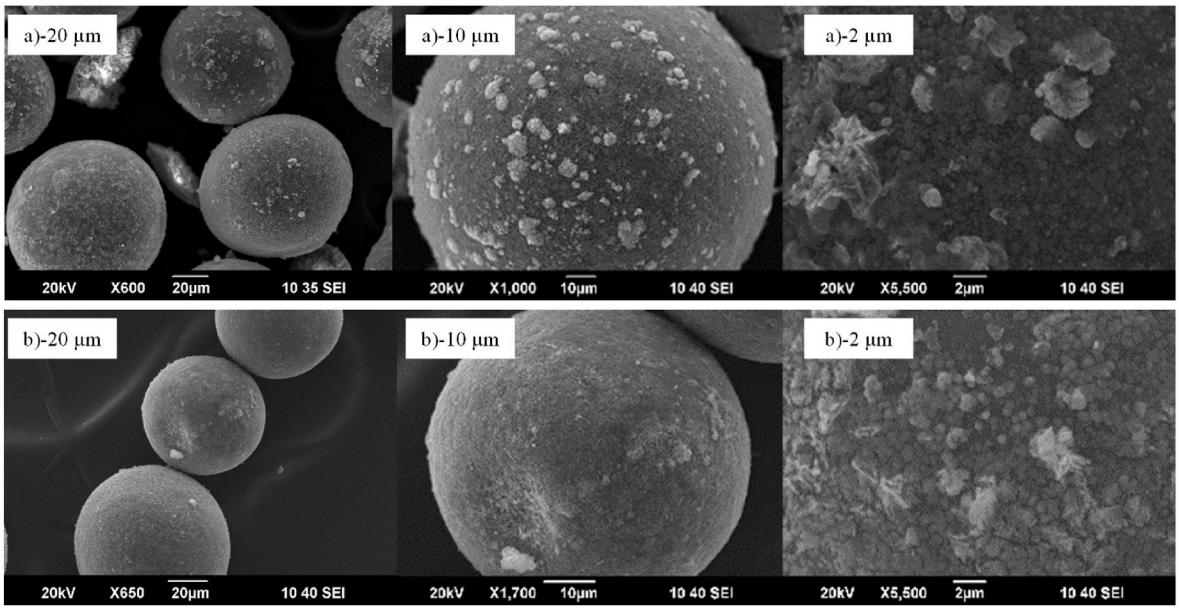

Fig. 9. SEM images of a) Co_3O_4/FCC and b) after hydrogen oxidation with Co_3O_4/FCC at 350 °C (CoO/FCC).

true densities of the new modified FCC support are presented in Table 2. The true density of the new metal oxide modified support are higher than the support itself. Since the true density of oxygen carriers, CuO (6.22 g/cm^3), Co_3O_4 (6.11 g/cm^3), and Mn_2O_3 (4.84 g/cm^3) are significantly higher compared to the true density of FCC support (2.70 g/cm^3). Thanks to the high ratio of FCC support in the oxidised oxygen carrier modified (13 wt % of CuO, 18 wt % of Co_3O_4, and 30 wt % of Mn_2O_3), the densities are close to the density of un-modified FCC support. The ratio of oxidised metal oxides impregnated FCC particles were theoretically calculated using the weight differences of FCC supports before and after the modification process. According to these calculations, approximately 12.5 wt% of CuO, 17.8 wt% of Co_3O_4 and 29.8 wt% of Mn_2O_3 were impregnated on the spent FCC particles. Additionally, the actual percentage of oxidised oxygen carriers impregnated on FCC particles measured by XRF and the results demonstrate values similar to the theoretical calculations, as seen in Table 2.

EDS mappings and qualitative element spectrums for CuO/FCC, Co_3O_4/FCC, and Mn_2O_3/FCC are presented in Fig. 12a and b, 12c-d, and 12e-f, respectively. The qualitative element spectrums after hydrogen oxidation are presented in Fig. 13a–d. The locations for qualitative element analysis of fresh and used metal oxide are shown on the SEM images using a rectangular (□) and plus (+) signs and presented as EDS spectrums next to the figures. Fig. 12a and b demonstrates that CuO were dispersed on the FCC support surface as observed Cu-mapping for CuO/FCC.

The EDS spectrums (Fig. 12a1-a4) proved that the intensity of CuO was not the same everywhere on the FCC particle surface, which could be attributed to CuO accumulation on the FCC support. CuO tends to concentrate on the exterior of a particle [24]. Furthermore, the surface accumulation of CuO increased with a rise in the CuO content. The EDS spectrums also demonstrate that fresh CuO/FCC consists of mainly Al, Si, O, and La in addition to Cu, which was impregnated on FCC as a form

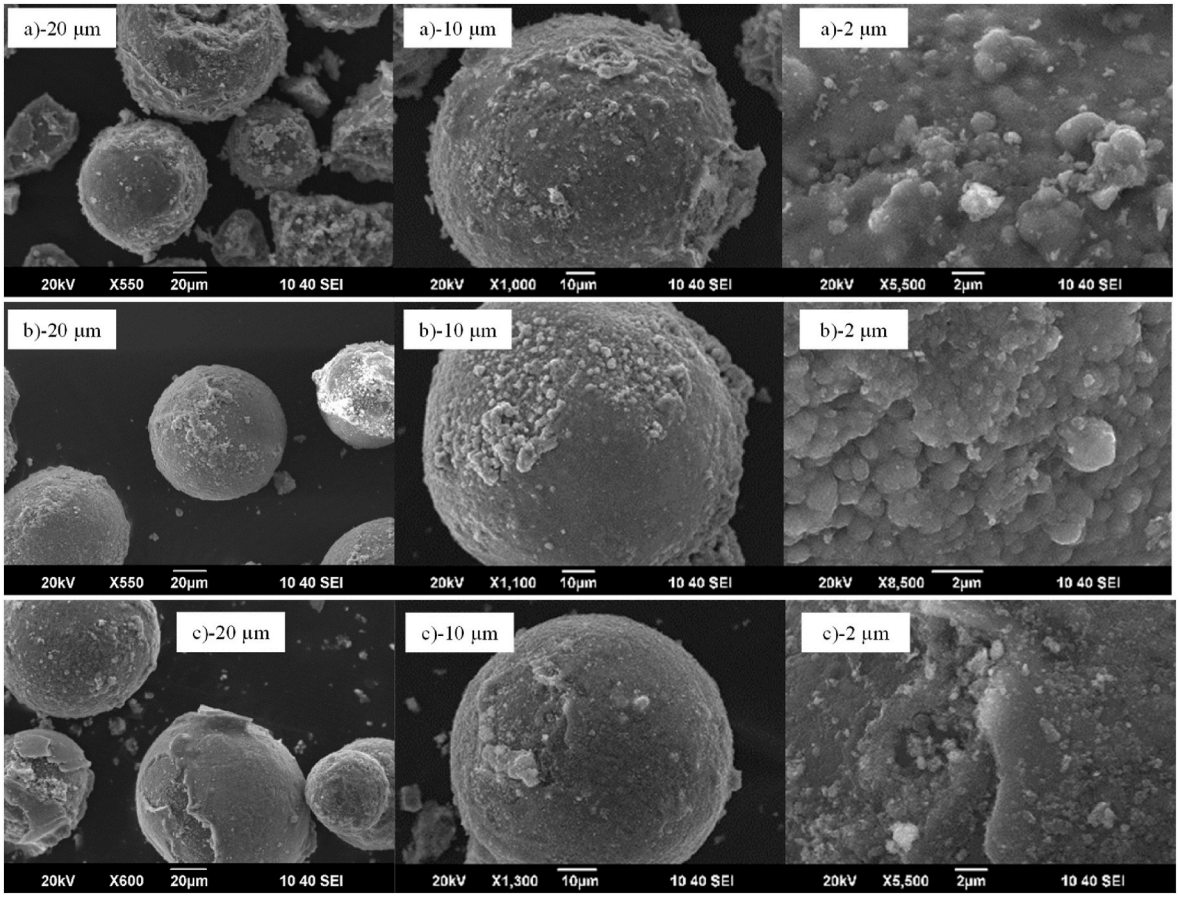

Fig. 10. SEM images of a) Mn_2O_3/FCC, b) hydrogen oxidation with Mn_2O_3/FCC at 300 °C (Mn_3O_4/FCC), and c) hydrogen oxidation with Mn_2O_3/FCC at 450 °C (MnO/FCC).

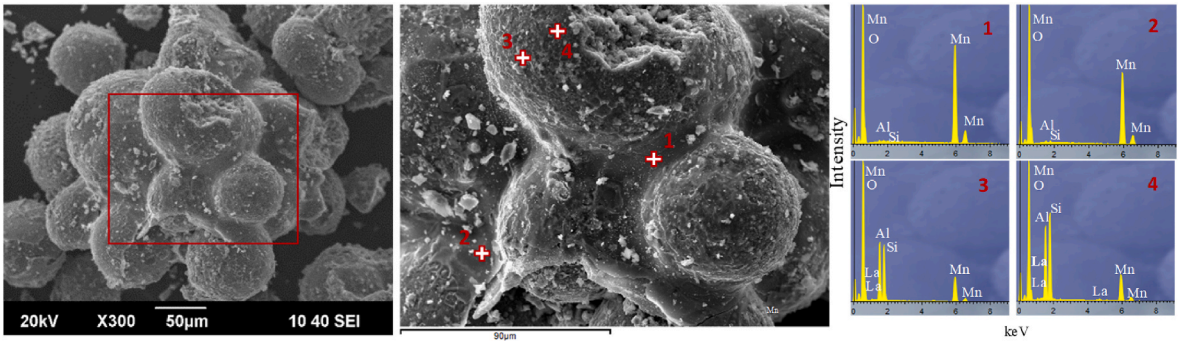

Fig. 11. SEM image and EDS spectrum of agglomerated part of fresh Mn_2O_3/FCC.

of CuO. The spectrums prove that the elements (Al, Si, La, O) creating FCC particles were remaining after impregnation of CuO.

Thanks to the preparation method of CuO/FCC, Co_3O_4/FCC, Mn_2O_3/FCC, the dispersion of reduced oxygen carriers on the FCC particles surface after hydrogen oxidation was expected to be the same with their oxidised states impregnated. As it can be detected on each elemental analysis, Cu was dispersed on the surface of FCC particles demonstrates in Fig. 13a. However, an accumulation of Cu was clearly observed on spot-2 in Fig. 13-a2 as similar with its oxidised forms on spot-2 in Fig. 12-a2. Fig. 12c and d demonstrates EDS Co-mapping and qualitative element analysis results for fresh and used Co_3O_4/FCC. A Co_3O_4 accumulation was observed over fresh Co_3O_4/FCC (Fig. 12c and d), whereas the used catalyst demonstrated better Co dispersion on the FCC support surface shown in Fig. 12d. The EDS spectrums clarify that the main elements, Al, Si, O, and La, are clearly measured with an additional metal (Co, which was impregnated on FCC support as a form of Co_3O_4). Additionally, Co peaks in Fig. 12c1-c3 are more intensive than the Cu peaks in Fig. 12a1-a4 as the amount of Co_3O_4 impregnated on FCC was higher than that of CuO impregnated on FCC.

The similar accumulation can also be observed on the reduced form of CoO in spot-2 and spot-4 in Fig. 13a2 and a4. Fig. 12e and f demonstrate that the impregnated Mn covers whole surface of the FCC particle as a layer, and this was not changed after the particle were used in the hydrogen oxidation (Fig. 13c and d). The dispersion of Mn, therefore, seems quite homogenous on both fresh and used Mn_2O_3/FCC due to this accumulation. Similarly, an apparent accumulation of MnO and Mn_3O_4 can be obtained from the SEM images of Mn_3O_4/FCC (Fig. 13c) and MnO/FCC (Fig. 13d). Additionally, the EDS spectrums

Table 2
Quantities and densities of metal oxides modified FCC support before and after hydrogen oxidation.

Oxygen carriers	Oxygen Carrier Phase	True density (g/cm^3)	Theoretical loading (wt.%)	Actual loading (wt.%)
FCC particle	n.a.	2.70	n.a.	n.a.
CuO/FCC	CuO	2.84	12.5	12.2
CuO/FCC (350 °C)	CuO → Cu	2.77	5.4	6.6
Co_3O_4/FCC	Co_3O_4	2.95	17.8	16.6
Co_3O_4/FCC (350 °C)	Co_3O_4 → CoO + Co	2.94	16.8	16.3
Mn_2O_3/FCC	Mn_2O_3	3.11	29.8	30.2
Mn_2O_3/FCC (300 °C)	Mn_2O_3 → Mn_3O_4 + MnO	3.05	29.0	29.4
Mn_2O_3/FCC (450 °C)	Mn_2O_3 → MnO	3.09	27.7	26.7

demonstrate a various intensity of Si and Al peaks on different spots (Fig. 12e1-e4), which also supported the intensive accumulation of Mn_2O_3 on the FCC particle surface. As mentioned previously, the accumulation of fresh oxygen carriers impregnated supports may be attributed to either cation states as Me^{3+} (such as Mn^{3+} and Co^{3+}) which may not be diffused into the pores of FCC particles while Me^{2+} (such as Cu^{2+} and Co^{2+}) can be placed into the pores or the preparation procedure where high amount of oxygen carriers were impregnated on FCC. The accumulation problem due to the cations Cu^{2+} and Co^{2+} may be decreased using multiple impregnation stages of CuO and Co_3O_4, as suggested by Chuang et al. [24] where the accumulation and agglomeration problems were not an issue for the preparation of CuO/Al_2O_3. Additionally, the other elements in the structure of FCC supports such as Si, Al, O and even La (trace amount) can still be detectable. Consequently, the reduced oxygen carriers Cu, CoO, MnO and Mn_3O_4 were not completely blocked the pores of FCC particles, which were still accessible for the oxidation of hydrogen.

4.4. N_2 adsorption-desorption analysis of oxygen carriers before and after reduction

The N_2 sorption isotherms of oxidised oxygen carriers modified FCC supports (CuO/FCC, Co_3O_4/FCC, Mn_2O_3/FCC) and after hydrogen oxidation at various temperatures are presented in Fig. 14. Adsorption and desorption isotherms of porous materials demonstrated different trends defined as hysteresis starting from about $P/P_0 = 0.4$, as seen in Fig. 14. According to the IUPAC classification [28,29], the isotherm is defined as "type IV", which is a typical isotherm of mesoporous materials having a pore diameter of 2–50 nm. As clearly seen from Fig. 14a that the adsorption-desorption isotherm of FCC support was the same even after the impregnation of oxidised oxygen carriers (CuO/FCC, Co_3O_4/FCC, Mn_2O_3/FCC). The reduced oxygen carriers (CuO/FCC at 350 °C, Co_3O_4/FCC at 350 °C, Mn_2O_3/FCC at 300 and 450 °C) did not change the FCC support sorption isotherms after hydrogen oxidation (Fig. 14b). The isotherms demonstrates two regions; the first one is monolayer/multilayer adsorption which is $P/P_0 = 0$–0.4 and the second

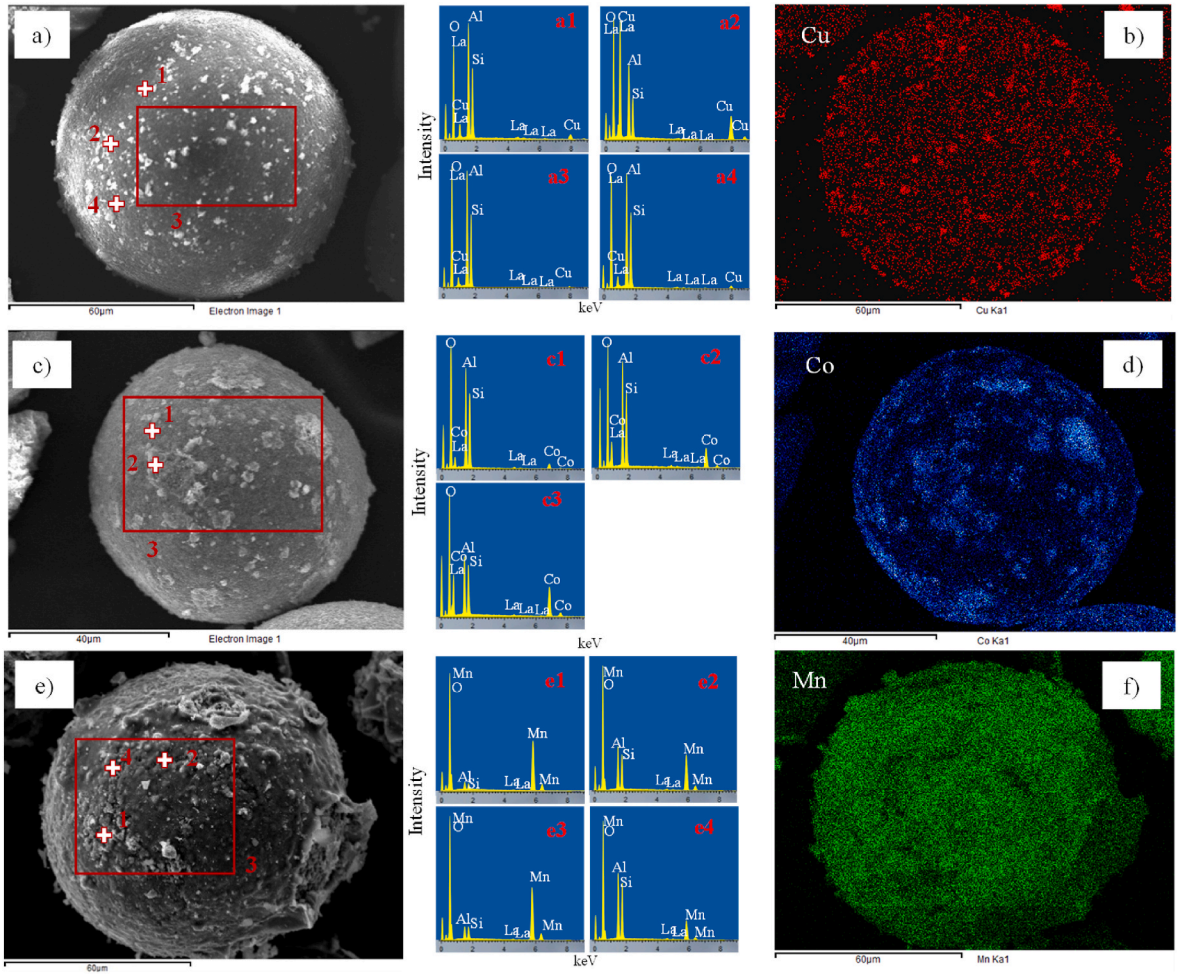

Fig. 12. EDS mapping and element spectrums for a-b) CuO/FCC, c-d) Co_3O_4/FCC, e-f) Mn_2O_3/FCC.

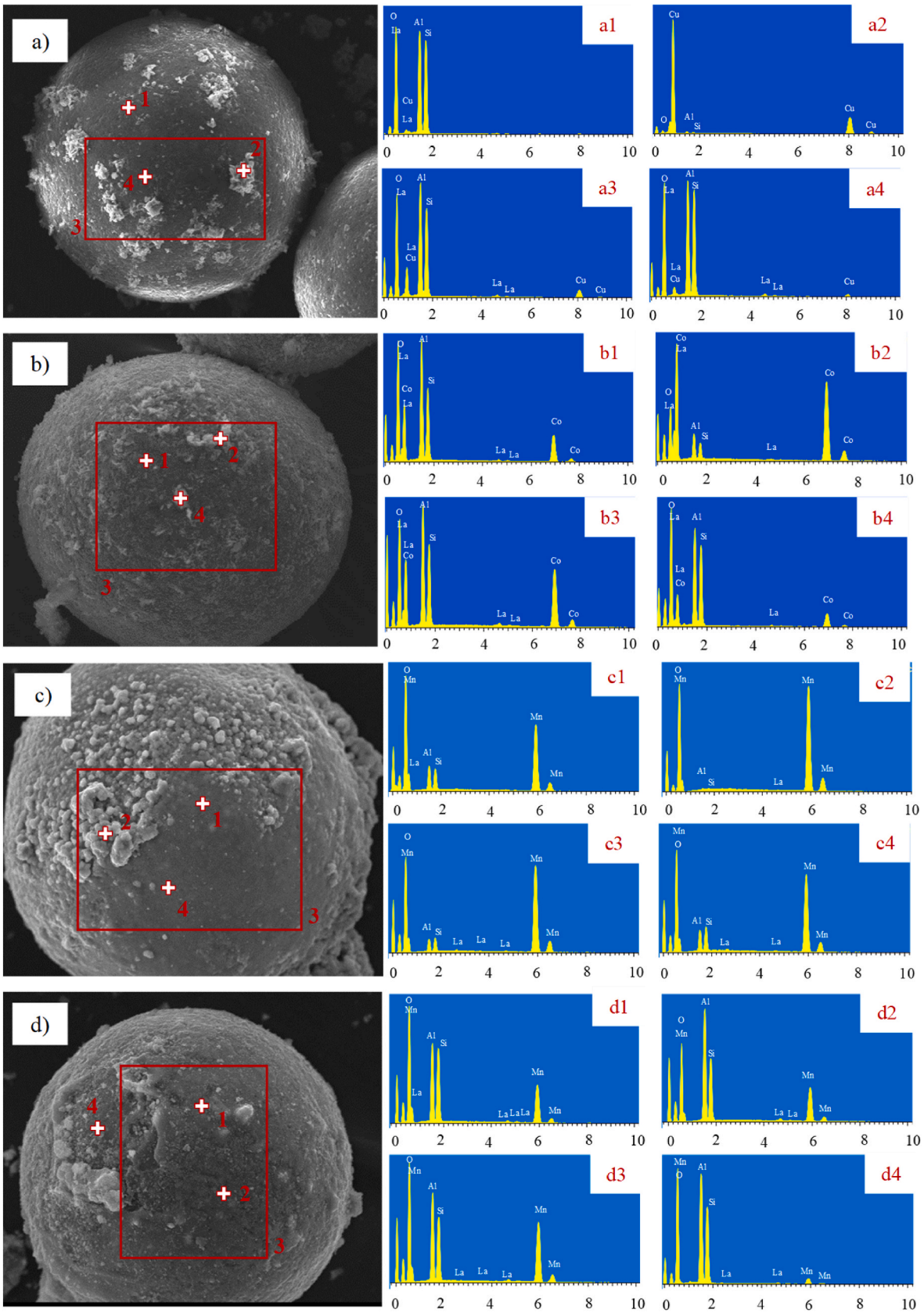

Fig. 13. EDS mapping and element spectrums after hydrogen oxidation with a) CuO/FCC at 350 °C (Cu/FCC). b) Co_3O_4/FCC at 350 °C (CoO/FCC), c) Mn_2O_3/FCC at 300 °C (MnO/Mn_3O_4/FCC), and d) Mn_2O_3/FCC at 450 °C (MnO/FCC).

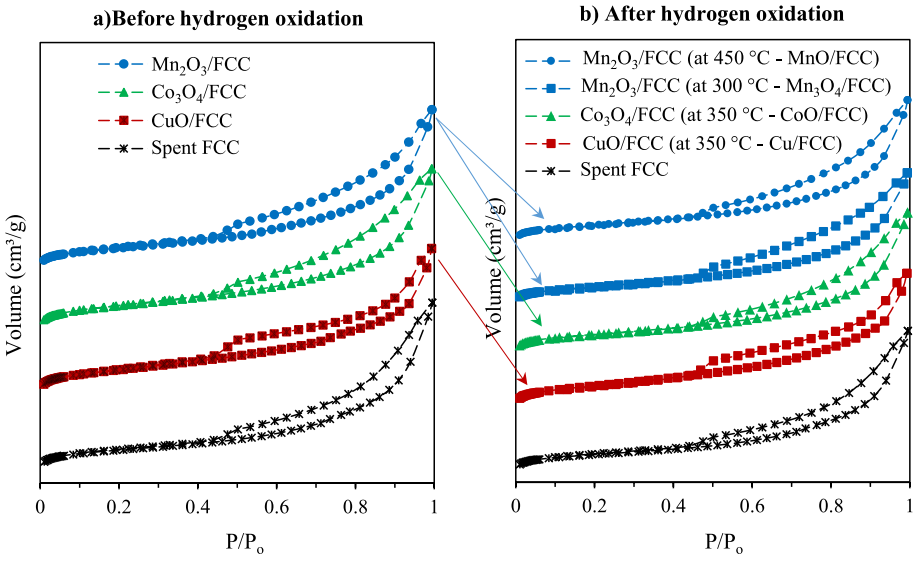

Fig. 14. Nitrogen adsorption-desorption isotherms of oxygen carriers supported by spent FCC supports; a) before and b) after hydrogen oxidation.

region is capillary condensation which represents with the hysteresis between adsorption-desorption lines ($P/P_0 = 0.5–0.99$) [28,29].

The textural properties of these oxygen carriers, such as pore structures (volume and diameter) and surface area were determined using Barrett-Joyner-Halenda (BJH) and Brunauer-Emmett-Teller (BET) methods (Table 3), respectively. The BET surface area slightly decreased by about 2, 6 and 14 m^2/g, following CuO, Co_3O_4 and Mn_2O_3 impregnation. This decrease is attributed to the concentration of oxidised metal oxide modification on FCC support, and these oxygen carriers could have filled the pores of the catalyst and blocked some of the surfaces. As the higher metal oxide concentration (CuO – 12.5 wt% < Co_3O_4 – 17.8 wt% < Mn_2O_3 – 29.8 wt%) resulted lower surface area (CuO – 189 m^2/g > Co_3O_4 – 185 m^2/g > Mn_2O_3 – 177 m^2/g). In terms of pore volume and average pore diameter, a clear decrease can also be observed after the impregnation of oxidised oxygen carriers, as demonstrated in Table 3. Similarly, the decreasing trend was also observed for the micropore volume with the increase in the concentration of impregnated oxidised oxygen carriers. Lower pore volume and surface area were also observed with the increasing of CuO ratio in modified ZSM-5 zeolite catalyst [27,30,31]. Similarly, Awayssa et al. [32] showed that the BET surface area decreased with the impregnation of Mn, and that a further decrease was observed once the Mn concentration increased. In another study, Du et al. [33] demonstrated that impregnation of different metals such as Co, Cu, Fe, Ga, Mo and Ni on ZSM-5 zeolite catalyst caused different levels of decrease in the surface area.

After hydrogen oxidation, BET surface area decreased, 10 m^2/g for the CuO/FCC reduction at 350 °C, 4 m^2/g for Co_3O_4/FCC reduction at 350 °C, 8 m^2/g for Mn_2O_3/FCC reduction at 300 °C as seen in Table 3. The reduction of Cuo to Cu, Co_3O_4 to CoO, and Mn_2O_3 to Mn_3O_4 with hydrogen decreased the micro surface area from 124 to 116 m^2/g, 107 to 103 m^2/g, 84 to 74 m^2/g, respectively. Furthermore, the reduction of oxidised oxygen carrier using hydrogen had no significant effect on the total pore volume as it was found around ~0.18 cm^3/g before and ~0.19 cm^3/g after hydrogen oxidation. The internal diffusion of metal oxides into the FCC support pores may results a decrease in the surface area, pore volume and diameter due to metal encapsulation and/or plugging over the surface and pores. Similarly, the BET surface area decreased with the impregnation of Mn and the further decrease was observed once the Mn concentration increased [32]. In another study, impregnation of different metals such as Co, Cu, Fe, Ga, Mo and Ni on ZSM-5 zeolite catalyst caused different levels in the surface area decrease [33].

4.5. Reduction stages of metal oxides

The characterisations before and after hydrogen oxidation via metal oxides in the previous sections (4.1, 4.2, 4.3, and 4.4) show that the oxidised CuO/FCC can be completely reduced to Cu/FCC (Reaction 4) with hydrogen at any temperature between 200 and 450 °C (Table 1), which propose a direct reduction from CuO to Cu instead of a sequential reduction steps as CuO → Cu_4O_3 → Cu_2O → Cu. However, Co_3O_4/FCC can be partially reduced to CoO/FCC (Reaction 5) and Co/FCC (Reactions 6–7) with hydrogen at 350 °C (the percentage of CoO was approximately 80.2% with a small portion of Co, 19.8%, Table 1), which may refer to a sequential reduction step Co_3O_4→CoO→Co at 300–450 °C. The increase in the operating temperature increase the

Table 3
Surface properties of metal oxides impregnated FCC before and after hydrogen oxidation.

Oxygen carriers	Oxygen Carrier Phase	Surface area (m^2/g)		Pore volume (cm^3/g)			Pore diameter (nm)	
		S_{BET}	S_{micro}	V_{tot}	V_{meso}	V_{micro}	d_{av}	d_{neck}
FCC particle	n.a.	191	102	0.25	0.20	0.05	13.8	11.0
CuO/FCC	CuO	189	124	0.18	0.14	0.04	11.9	10.5
CuO/FCC (350 °C)	CuO → Cu	179	116	0.19	0.15	0.04	13.0	10.3
Co_3O_4/FCC	Co_3O_4	185	107	0.18	0.15	0.03	13.2	9.6
Co_3O_4/FCC (350 °C)	Co_3O_4 → CoO + Co	181	103	0.19	0.16	0.03	13.5	10.2
Mn_2O_3/FCC	Mn_2O_3	177	84	0.17	0.15	0.02	12.5	10.0
Mn_2O_3/FCC (300 °C)	Mn_2O_3 → Mn_3O_4 + MnO	169	74	0.17	0.15	0.02	12.8	8.8
Mn_2O_3/FCC (450 °C)	Mn_2O_3 → MnO	177	87	0.18	0.17	0.01	13.7	10.0

reduction kinetics and produce more Co less CoO. Furthermore, the potential reduction mechanisms of Mn_2O_3/FCC could be a complete/partial reduction to Mn_3O_4/FCC (Reaction 8) at 250 °C or MnO/FCC (Reaction 9–10) at 450 °C.

CuO reduction by hydrogen oxidation

$$CuO + H_2 \rightarrow Cu + H_2O \quad (R4)$$

Co_3O_4 reduction by hydrogen oxidation

$$Co_3O_4 + H_2 \rightarrow 3CoO + H_2O \quad (R5)$$

$$Co_3O_4 + 8H_2 \rightarrow 3Co + 4H_2O \quad (R6)$$

$$CoO + H_2 \rightarrow 3Co + H_2O \quad (R7)$$

Mn_2O_3 reduction by hydrogen oxidation

$$3Mn_2O_3 + H_2 \rightarrow 2Mn_3O_4 + H_2O \quad (R8)$$

$$Mn_2O_3 + H_2 \rightarrow 2MnO + H_2O \quad (R9)$$

$$Mn_3O_4 + H_2 \rightarrow 3MnO + H_2O \quad (R10)$$

5. Conclusions

This study presents the applicability of low-temperature oxidation of hydrogen with chemical looping technology with three different metal oxides: CuO, Mn_2O_3 and Co_3O_4. The comprehensive characterisations of oxygen carriers before and after hydrogen oxidation provided insightful knowledge on the understanding of the potential reduction stages of metal oxides and the oxidation mechanism of hydrogen at low temperatures.

- The metal oxides (CuO, Co_3O_4, Mn_3O_4) were successfully impregnated over the spent FCC catalysts at various ratios of 10–30 wt%.
- The higher quantity of metal oxide (Mn_3O_4) impregnation resulted in clear accumulation over the external surface of FCC support like a 'blanket', whereas the surface characterisations (i.e. surface area and pore structures) did not show a significant change.
- CuO directly reduced to Cu (CuO→Cu), instead of following a sequential reduction step CuO→Cu_4O_3→Cu_2O→Cu at the temperatures of 200–450 °C.
- Co_3O_4 was reduced to a mixture CoO and Co at various temperatures of 200–450 °C referring to the sequential reduction steps of Co_3O_4→CoO→Co.
- Mn_2O_3 can also reduce to a mixture of Mn_3O_4 and MnO at temperatures between 250 and 400 °C, which also refers a sequential reduction of Mn_2O_3→Mn_3O_4→MnO.

Based on the experimental results, low-temperature CLC could be an applicable method for safe and flameless hydrogen combustion while it produces the heat required for space heating. As future work, a comprehensive investigation of different metal oxides at low-temperature chemical looping oxidation of hydrogen would be investigated with Density Function Theory (DFT). The reduction mechanisms of different oxygen carriers and kinetics of these reduction reactions would be able to assess the technology for the preparation of different metal composites and the potential applications of these metal composites in thermochemical energy storage. A detailed techno-economic analysis with an appropriate scale could also shows how this technology compatible with space heating.

Declaration of competing interestd

The authors declare that they have no known competing financial interests or personal relationships that could have appeared to influence the work reported in this paper.

Acknowledgements

This research was funded and supported by University of Nottingham under "FPVC Research Acceleration Fund" and "Advanced Materials Research Group (AMRG) Early Career Researcher Collaboration Fund". The authors also thank the Nanoscale and Microscale Research Centre (nmRC) for providing access to SEM instrumentation.

References

[1] A. Nandy, C. Loha, S. Gu, P. Sarkar, M.K. Karmakar, P.K. Chatterjee, Present status and overview of chemical looping combustion technology, Renew. Sustain. Energy Rev. 59 (2016) 597–619.
[2] J. Squires, A. Goater, Carbon Footprint of Heat Generation, POSTnote house of Parliament, Parliamentary Office of Science and Technology, 2016.
[3] K. Hansen, Decision-making based on energy costs: comparing levelized cost of energy and energy system costs, Energy Strategy Rev. 24 (2019) 68–82.
[4] H. Pawlak-Kruczek, A. Arora, K. Mościcki, K. Krochmalny, S. Sharma, L. Niedzwiecki, A transition of a domestic boiler from coal to biomass–Emissions from combustion of raw and torrefied Palm Kernel shells (PKS), Fuel 263 (2020), 116718.
[5] BEIS, Boilers: Hot Water, Biomass and Steam; A Guide to Energy Efficient Equipment Listed on the Energy Technology List (ETL), The Department for Business, Energy & Industrial Strategy (BEIS), 2020.
[6] V. Singh, N. Chauhan, Fundamentals and use of hydrogen as a fuel, ISST Journal of Mechanical Engineering 6 (2015) 63.
[7] Z. Abdin, A. Zafaranloo, A. Rafiee, W. Mérida, W. Lipiński, K.R. Khalilpour, Hydrogen as an energy vector, Renew. Sustain. Energy Rev. 120 (2020), 109620.
[8] M. Ball, M. Wietschel, The future of hydrogen–opportunities and challenges, Int. J. Hydrogen Energy 34 (2) (2009) 615–627.
[9] S. Wang, L. Chen, F. Niu, D. Chen, L. Qin, X. Sun, Y. Huang, Catalytic combustion of hydrogen for residential heat supply application, Int. J. Energy Res. 40 (14) (2016) 1979–1985.
[10] A.E. Kozhukhova, S.P. du Preez, D.G. Bessarabov, Catalytic hydrogen combustion for domestic and safety applications: a critical review of catalyst materials and technologies, Energies 14 (16) (2021) 4897.
[11] L. Das, Hydrogen-fueled Internal Combustion Engines, Compendium of Hydrogen Energy, Elsevier, 2016, pp. 177–217.
[12] D.R. Jones, W.A. Al-Masry, C.W. Dunnill, Hydrogen-enriched natural gas as a domestic fuel: an analysis based on flash-back and blow-off limits for domestic natural gas appliances within the UK, Sustain. Energy Fuels 2 (4) (2018) 710–723.
[13] S. Chuang, J. Dennis, A. Hayhurst, S. Scott, Kinetics of the chemical looping oxidation of H2 by a co-precipitated mixture of CuO and Al2O3, Chem. Eng. Res. Des. 89 (9) (2011) 1511–1523.
[14] F. Güleç, W. Meredith, C.-G. Sun, C.E. Snape, Selective low temperature chemical looping combustion of higher alkanes with Cu-and Mn-oxides, Energy 173 (2019) 658–666.
[15] M. Noor, A.P. Wandel, T. Yusaf, The modelling of the effect of air fuel ratio on unburned hydrocarbons for MILD combustion, in: Proceedings of the 2nd Malaysian Postgraduate Conference (MPC 2012), Education Malaysia, Sydney (EMAS), 2012, pp. 159–163.
[16] L. Xu, Z. Li, H. Sun, J. Bao, N. Cai, Low-temperature chemical looping combustion for removing unburnt gaseous components with a cement-supported CuO oxygen carrier, Energy Fuel. 27 (11) (2013) 6872–6879.
[17] A.T. Atimtay, B. Kaynak, Co-combustion of peach and apricot stone with coal in a bubbling fluidized bed, Fuel Process. Technol. 89 (2) (2008) 183–197.
[18] W. Wei, S. Wang, S. Chatani, Z. Klimont, J. Cofala, J. Hao, Emission and speciation of non-methane volatile organic compounds from anthropogenic sources in China, Atmos. Environ. 42 (20) (2008) 4976–4988.
[19] R.N. Harper, C.M. Boyce, S.A. Scott, Oxygen carrier dispersion in inert packed beds to improve performance in chemical looping combustion, Chem. Eng. J. 234 (2013) 464–474.
[20] F. Güleç, W. Meredith, C.-G. Sun, C.E. Snape, A novel approach to CO2 capture in fluid catalytic cracking—chemical looping combustion, Fuel 244 (2019) 140–150.
[21] F. Güleç, W. Meredith, C.-G. Sun, C.E. Snape, Demonstrating the applicability of chemical looping combustion for the regeneration of fluid catalytic cracking catalysts, Chem. Eng. J. 389 (2020), 124492.
[22] J. Pike, S.-W. Chan, F. Zhang, X. Wang, J. Hanson, Formation of stable Cu2O from reduction of CuO nanoparticles, Appl. Catal. Gen. 303 (2) (2006) 273–277.
[23] M. Ward, E. Boyes, P. Gai, In-situ Reduction of Co3O4 in H2 Using Environmental HRTEM, Journal of Physics: Conference Series, IOP Publishing, 2014, 012009.
[24] S. Chuang, J. Dennis, A. Hayhurst, S. Scott, Development and performance of Cu-based oxygen carriers for chemical-looping combustion, Combust. Flame 154 (1–2) (2008) 109–121.
[25] L.F. De Diego, P. Gayán, F. García-Labiano, J. Celaya, A. Abad, J. Adánez, Impregnated CuO/Al2O3 oxygen carriers for chemical-looping combustion: avoiding fluidized bed agglomeration, Energy Fuel. 19 (5) (2005) 1850–1856.
[26] A. Bhan, W. Nicholas Delgass, Propane aromatization over HZSM-5 and Ga/HZSM-5 catalysts, Catal. Rev. 50 (1) (2008) 19–151.
[27] S. Wang, Q. Cai, J. Chen, L. Zhang, L. Zhu, Z. Luo, Co-cracking of bio-oil model compound mixtures and ethanol over different metal oxide-modified HZSM-5 catalysts, Fuel 160 (2015) 534–543.

[28] K.S. Sing, Reporting physisorption data for gas/solid systems with special reference to the determination of surface area and porosity (Recommendations 1984), Pure Appl. Chem. 57 (4) (1985) 603–619.
[29] M. Thommes, K. Kaneko, A.V. Neimark, J.P. Olivier, F. Rodriguez-Reinoso, J. Rouquerol, K.S. Sing, Physisorption of gases, with special reference to the evaluation of surface area and pore size distribution (IUPAC Technical Report), Pure Appl. Chem. 87 (9–10) (2015) 1051–1069.
[30] K. Kubo, H. Iida, S. Namba, A. Igarashi, Comparison of steaming stability of Cu-ZSM-5 with those of Ag-ZSM-5, P/H-ZSM-5, and H-ZSM-5 zeolites as naphtha cracking catalysts to produce light olefin at high temperatures, Appl. Catal. Gen. 489 (2015) 272–279.
[31] C. Li, J. Ma, Z. Xiao, S.B. Hector, R. Liu, S. Zuo, X. Xie, A. Zhang, H. Wu, Q. Liu, Catalytic cracking of Swida wilsoniana oil for hydrocarbon biofuel over Cu-modified ZSM-5 zeolite, Fuel 218 (2018) 59–66.
[32] O. Awayssa, N. Al-Yassir, A. Aitani, S. Al-Khattaf, Modified HZSM-5 as FCC additive for enhancing light olefins yield from catalytic cracking of VGO, Appl. Catal. Gen. 477 (2014) 172–183.
[33] Z. Du, X. Ma, Y. Li, P. Chen, Y. Liu, X. Lin, H. Lei, R. Ruan, Production of aromatic hydrocarbons by catalytic pyrolysis of microalgae with zeolites: catalyst screening in a pyroprobe, Bioresour. Technol. 139 (2013) 397–401.